**Supplementary Material**

for the manuscript

# 1.2-million-year band of Earth–Mars obliquity modulation on the evolution of cold late Miocene to warm early Pliocene climate

Jie Qin[1,2], Rui Zhang[1,2*], Vadim A. Kravchinsky[1,2,*], Jean-Pierre Valet[1,3], Leonardo Sagnotti[4], Jianxing Li[5], Yong Xu[6], Taslima Anwar[1,2], Leping Yue[1]

[1] Institute of Cenozoic Geology and Environment, State Key Laboratory of Continental Dynamics, Department of Geology, Northwest University, 710069 Xi'an, China

[2] Geophysics, Department of Physics, University of Alberta, T6G2E1 Edmonton, Canada

[3] Institut de Physique du Globe de Paris, 75238 Paris cedex 05, France

[4] Istituto Nazionale di Geofisica e Vulcanologia, 00143 Roma, Italy

[5] Chengdu Center of Geological Survey, Geological Survey of China, 610081 Chengdu, China

[6] Xi'an Center of Geological Survey, China Geological Survey, 710054 Xi'an, China

* Corresponding author emails: ruizhang@nwu.edu.cn; vadim@ualberta.ca

This PDF file includes:

## S1 - Introduction

The East Asian monsoon (EAM) system controls precipitation and dust accumulation by seasonal alternation of inputs of warm moist air from Indian Ocean and Pacific Ocean, and dry dust-bearing winds from the high latitudes and high altitudes, which resulted in the creation of the typical sedimentary sequence of the Chinese Loess Plateau (CLP). Heller and Liu (1982) built the robust chronology for the 2.5 Ma loess deposits. The age of underlain eolian red clay was first assigned to the Pliocene at 4 – 5 Ma (Evans et al., 1991; Zheng et al., 1992) and later to the late Miocene at ~7 – 8 Ma (Ding et al., 1998, Sun et al., 1998a, b), the early Miocene at 22 Ma (Guo et al., 2002) and the late Oligocene at 25 Ma (Qiang et al., 2011). Recent magnetostratigraphic studies, however, raised a problem of inconsistency in the reconstructed chronology for the eolian red clay sections in the eastern CLP. For example, a debate exists about the dating of the Jiaxian section where Ding et al. (1998) considered its deposition started at 5.2 Ma and Qiang et al. (2001) considered it started at 7.2 Ma. Another example of inconsistent age assignments refers to the age of the bottom of the Shilou (SL) section: it was first determined as 11 Ma (Xu et al., 2009), then 5.2 Ma (Anwar et al., 2015) and 8 Ma (Ao et al., 2016). Visual correlation of identified magnetic polarity intervals to the Geomagnetic Polarity Time Scale (GPTS), in the case of the lack of other independent chronostratigraphic constraints, can potentially produce different outcomes, especially when short polarity intervals are considered as geomagnetic subchrons, excursions and tiny wiggles, and even remagnetization (by the groundwater in this study). As a significant improvement in data analysis, the detection of astronomical signals in cyclostratigraphy has provided impressive advancements in stratigraphic correlations, by adjusting the magnetostratigraphic patterns through matching stratigraphic records to the Earth's orbital periodicities typical of the Milankovitch cycles (Anwar et al., 2015; Zhang et al., 2018, 2021a, 2021b, 2022).

## S2 - Stratigraphic correlations from eastern to western CLP

We compare the LL section to two other classical sections in the eastern and western edges of CLP, in a time interval spanning across the Mio-Pliocene boundary (Supplementary Material Fig. 1). Both Baode (BD) and Dongwan (DW) sections are located close to the mountains (for example, DW is located between Liupan Mts and West Qinling Mts which is close to Tibetan Plateau) as well as LL and SL (Hao and Guo, 2004; Zhu et al., 2008; Xu et al., 2009). These sections might be more affected by the seasonal cyclic variations of the Asian monsoon driven by tectonic uplift of a series of mountains during the Mio-Pliocene climate transition (Anwar et al., 2015; Zhang et al., 2021b; Zhang et al., 2022).

The lower part of the LL section, between 30–68 m, corresponds to the 38–69 m interval in the DW section and to of 60–117 m interval in the BD section, characterized by low MS values (average of 38 × $10^{-8}$ $m^3$/kg for Liulin, 64 × $10^{-8}$ $m^3$/kg for DW, 59 × $10^{-8}$ $m^3$/kg for BD) and wide oscillations (Supplementary Material Fig. 1a). The upper part of the LL section between 0–30 m correlates to the interval of 12–38 m in DW and with interval of 49–60 m in BD, characterized by distinctly higher MS values (average of 57 × $10^{-8}$ $m^3$/kg for LL, 123 × $10^{-8}$ $m^3$/kg for BD, 107 × $10^{-8}$ $m^3$/kg for DW) and lower amplitude oscillations. The MS variations for each section in the reconstructed time framework are shown in Supplementary Material Fig. 1b. Two stages can be recognized across the LL section: the first stage at depth of 0 – 30 m represents the time interval of 5.5 – 4 Ma and the second stage at the depth of 30 – 68 m represents the time interval of 7 – 5.5 Ma. These data indicate that MS trend reflects a climate transition from lower values with stronger oscillations to higher values with slighter oscillations, while the trend of the coarse fraction (>63 μm) content shows a corresponding transition at 30 m (ca. 5.5 Ma), from high values with wide variations in the lower part to low values with limited variations in the upper part (Supplementary Material Fig. 1). Both MS and GS trends suggest a transition for the Asian atmospheric circulation around the MPB boundary, a shift in the monsoon regime from the strengthening winter and weakening summer to the weakening winter and strengthening summer. This shift is synchronous with the DW section (Hao and Guo, 2004; Li et al., 2008), whereas it appears slightly younger (5.3 Ma) in the BD section (Zhu et al., 2008).

## S3 - Wavelet analysis of magnetic susceptibility in the central CLP

In the past few decades, many studies on successive red clay sections have been conducted through the CLP. Most chronology has been extensively studied and constrained through magnetostratigraphy ((Heller et al., 1982; Ding et al., 1998; Hao and Guo, 2004; Vandenberghe et al., 2004; Ao et al., 2016). In the main text, we compare the Jingchuan red clay section (Ding et al., 2001) from the middle part of CLP with LL and SL from eastern CLP. We show clearly the 1.2 Myr obliquity grand cycle observed in these sections. Further, here we integrated the other two well-constrained sections from the heart of CLP, to obtain a composite record of MS signal and Asian monsoon variability. These are Chaona (CN, Song et al., 2007, 2018) and Lingtai (LT, Ding et al., 1999; Sun et al., 2010), from the central CLP (Supplementary Material

Fig. 2). The wavelet of MS from above sections, including a stacked MS, documented the amplitude-modulated 1.2 Myr band superimposed on the obliquity and eccentricity cycles for the first time discovery (Supplementary Material Fig. 3).

For stacked magnetic susceptibility (SMS) from LT, CN and JC sections in the central CLP, we started with aligning these records using a graphic correlation technique (Lisiecki and Lisiecki, 2002). Automated correlation algorithms (Lisiecki & Raymo, 2005) provided the first alignment criteria of objective technique to achieve a peak by peak correlation. Each alignment step was also evaluated by stratigraphic features to determine the quality of the matching and to distinguish noise or add tie points. We then chose the age model of one section (herein, LT) as a reference signal to correlate. Each MS record was aligned to the target and then averaged the normalized data at each time level to obtain the initial stacked data. After creating the initial stack, we tuned it to the 1.2-Myr-filtering obliquity as the prominent cycles were visually observed across all these sections (Supplementary Material Fig. 2). The process was iterative, for each result we monitored the spectral presence, if no good orbital cycles showed, we returned to the first step.

**References**


Ao, H., Roberts, A. P., Dekkers, M. J., Liu, X., Rohling, E. J., Shi, Z., An, Z. and Zhao, X., 2016. Late Miocene–Pliocene Asian monsoon intensification linked to Antarctic ice-sheet growth. Earth and Planetary Science Letters 444, 75–87.

Ding, Z., Sun, J., Liu, T., Zhu, R., Yang, S. and Guo, B., 1998. Wind-blown origin of the Pliocene red clay formation in the central Loess Plateau, China. Earth and Planetary Science Letters 161, 135–143.

Ding, Z., Xiong, S., Sun, J., Yang, S., Gu, Z. and Liu, T., 1999. Pedostratigraphy and paleomagnetism of a ~7.0 Ma eolian loess-red clay sequence at Lingtai, Loess Plateau, north-central China and the implications for paleomonsoon evolution. Palaeogeography, Palaeoclimatology, Palaeoecology 152, 49–66.

Ding, Z., Yang, S., Hou, S., Wang, X., Chen, Z. and Liu, T., 2001. Magnetostratigraphy and sedimentology of the Jingchuan red clay section and correlation of the Tertiary eolian red clay sediments of the Chinese Loess Plateau. Journal of Geophysical Research: Solid Earth 106, 6399–6407.

Hao, Q., Guo, Z., 2004. Magnetostratigraphy of a late Miocene-Pliocene loess-soil sequence in the western Loess Plateau in China. Geophysical Research Letters 31.

Heller, F., Tung-sheng, L., 1982. Magnetostratigraphical dating of loess deposits in China. Nature 300, 431-433. https://xs.scihub.ltd/https://doi.org/10.1038/300431a0.

Lisiecki, L. E., Lisiecki, P. A., 2002. Application of dynamic programming to the correlation of paleoclimate records. *Paleoceanography*, *17*, 1–1.

Lisiecki, L. E., Raymo, M. E., 2005. A Pliocene - Pleistocene stack of 57 globally distributed benthic δ18O records. *Paleoceanography*, *20*.

Song, Y., Fang, X., Chen, X., Torii, M., Ishikawa, N., Zhang, M., Yang, S. and Chang., 2018. Rock magnetic record of late Neogene red clay sediments from the Chinese Loess Plateau and its implications for East Asian monsoon evolution. Palaeogeography, Palaeoclimatology, Palaeoecology 510, 109–123.

Song, Y., Fang, X., Torii, M., Ishikawa, N., Li, J. and An, Z., 2007. Late Neogene rock magnetic record of climatic variation from Chinese eolian sediments related to uplift of the Tibetan Plateau. Journal of Asian Earth Sciences 30, 324–332.

Sun, Y., An, Z., Clemens, S. C., Bloemendal, J., Vandenberghe, J., 2010. Seven million years of wind and precipitation variability on the Chinese Loess Plateau. Earth and Planetary Science Letters 297, 525–535.

Vandenberghe, J., Lu, H., Sun, D., van Huissteden, J.K., Konert, M., 2004. The late Miocene and Pliocene climate in East Asia as recorded by grain size and magnetic susceptibility of the Red Clay deposits (Chinese Loess Plateau). Palaeogeography, Palaeoclimatology, Palaeoecology 204, 239-255.

Zhang, R., Kravchinsky, V. A., Anwar, T., Yue, L., Li, J. and Jiao, J., 2018. Comment on" Late Miocene-Pliocene Asian monsoon intensification linked to Antarctic ice-sheet growth"[Earth Planet. Sci. Lett. 444 (2016) 75-87]. Earth and Planetary Science Letters 503, 248–251.

Zhang, R., Kravchinsky, V. A., Qin, J., Goguitchaichvili, A., Li, J., 2021a. One and a Half Million Yearlong Aridity During the Middle Eocene in North-West China Linked to a Global Coooling Episode. *Journal of Geophysical Research: Solid Earth 126*, e2020JB021037.

Zhang, R., Wei, X., Kravchinsky, V. A., Yue, L., Zheng, Y., Qin, J., Yang, L., Ma, M., Xian, F., Gong, H., Zhang, Y., Liu, X., 2021b. “Tiny wiggles” in the late Miocene red clay deposits in the north-east of the Tibetan Plateau. Geophysical Research Letters, 48, e2021GL093962.

Zhang, R., Li, X., Xu, Y., Li, J., Sun, L., Yue, L., Pan, F., Xian, F., Wei, X., Cao, Y., 2022. The 173-kyr obliquity cycle pacing the Asian monsoon in the eastern Chinese Loess Plateau from late Miocene to Pliocene. Geophysical Research Letters, 49, e2021GL097008.

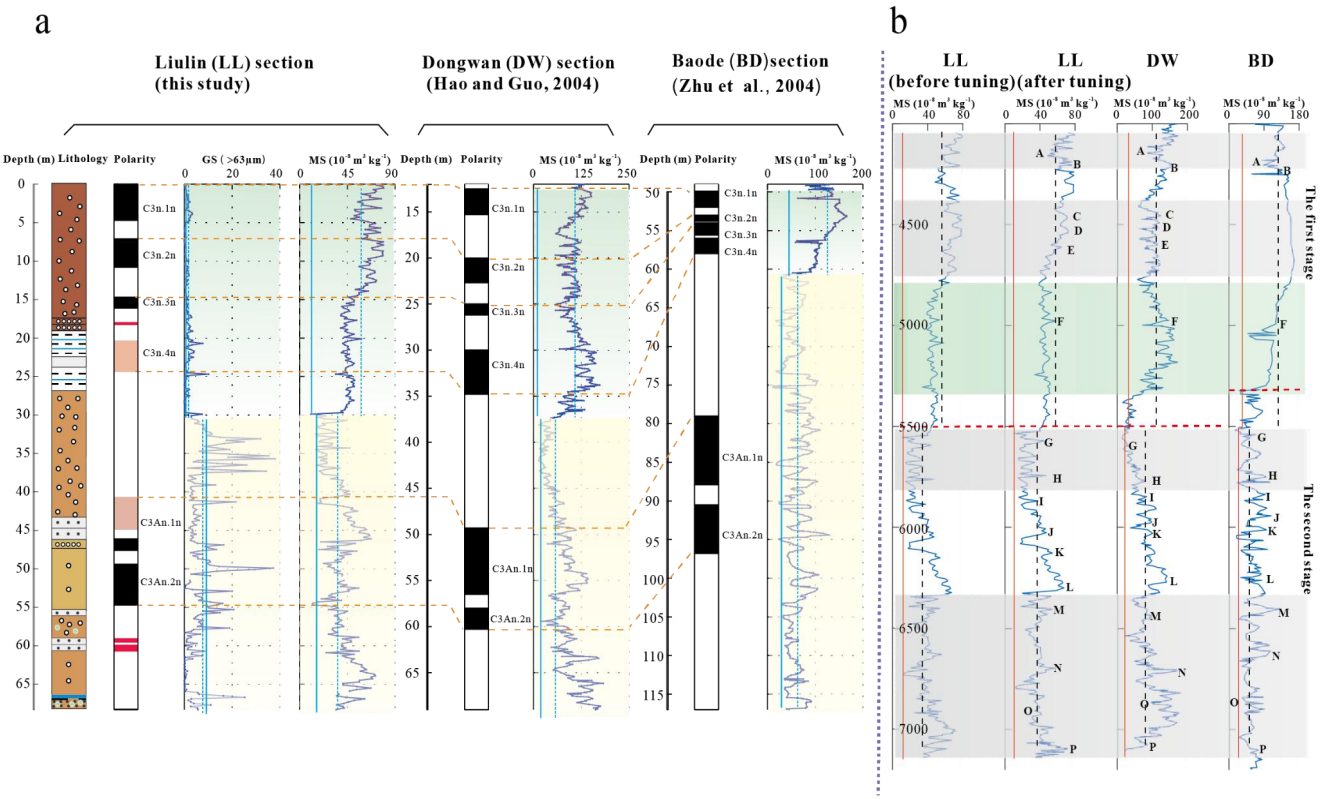


**Supplementary Material Fig. 1.** Comparison of polarity and magnetic susceptibility as a function of depth and age for the red clay sections. (a) LL: Polarity, grain size and MS of the LL red clay section. DW: Polarity and MS of the DW red clay section (Hao and Guo, 2002). BD: Polarity and MS of the BD red clay section (Zhu et al., 2008). The yellow dashed lines correlate the corresponding polarities of each section for mutual comparison. The green and yellow shadings indicate two comparable stages in changing MS for each section. Blue dashed lines represent the average values for each stage and blue solid lines represent the standard deviation. (b) Comparison of MS as a function of age for the red clay sections. LL: MS of the LL red clay section before tuning to eccentricity; MS of the LL red clay section after tuning to eccentricity. DW: MS of the DW red clay section. BD: MS of the BD red clay. The chronology for the DW and BD red clay sequences was obtained from magnetostratigraphy. The gray and white shadings indicate each comparable time interval of the three sections during which consistent variations can be observed. The red dashed lines denote the two stages reflecting different climatic conditions. The black dashed lines represent the average values of each stage and red solid lines represent the standard deviation. A–P shows consistent peaks from MS variations in the three sections during 7–4 Ma.

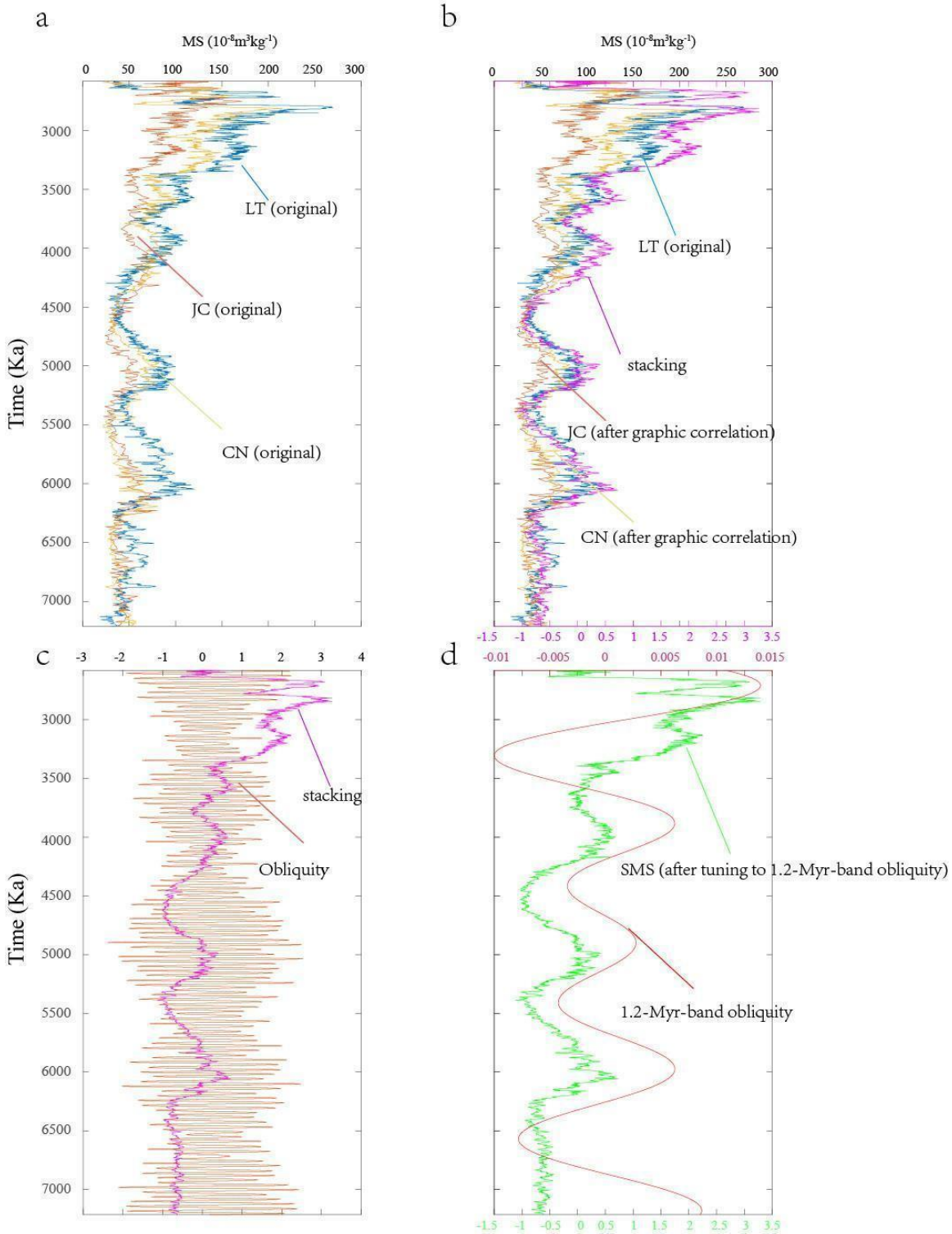


**Supplementary Material Fig. 2.** Illustration of stacking processing of magnetic susceptibility records from the central Chinese Loess Plateau. (a) Original magnetic susceptibility records before processing: blue–LT (Ding et al., 1999), yellow–JC (Ding et al., 2001), brown–CN (Song et al., 2007). (b) Magnetic susceptibility after graphic correlation and stacking. (c) Comparison of the initial stacking data and obliquity solution. (d) Stacked magnetic susceptibility after tuning to the 1.2-Myr-band obliquity.

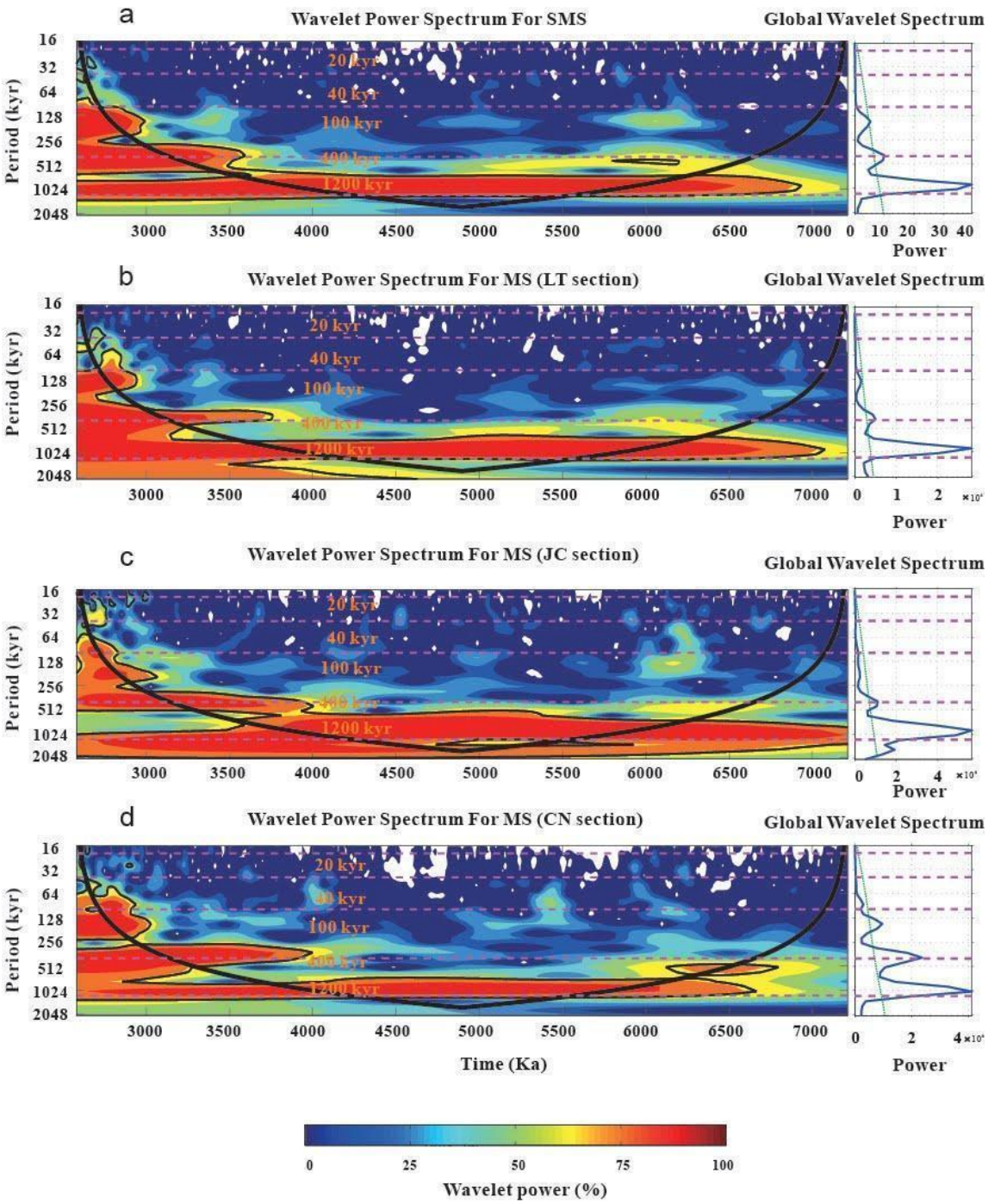


**Supplementary Material Fig. 3.** Wavelet analysis of magnetic susceptibility records from the central Chinese Loess Plateau. (a) Wavelet spectrum of the Sacked magnetic susceptibility. (b) Wavelet spectrum of magnetic susceptibility from the LT section. (c) Wavelet spectrum of magnetic susceptibility from the JC section. (d) Wavelet spectrum of magnetic susceptibility from the CN section. The purple dashed line marks the orbital period. The thin black contour encloses regions of greater than 95% confidence for a red-noise process with a lag coefficient of 0.8. The thick black contour indicates the cone of influence. The global wavelet spectrum to the right illustrates the mean red noise spectrum, as indicated by the green dashed line. The color bars correspond to wavelet power.